Competition between band topology and non-Hermiticity

Jiewei Cheng,[1,*] Xiujuan Zhang,[1,†] Ming-Hui Lu,[1,2,3,‡] and Yan-Feng Chen[1,3]
[1]*National Laboratory of Solid State Microstructures and Department of Materials Science and Engineering, Nanjing University, Nanjing 210093, China*
[2]*Jiangsu Key Laboratory of Artificial Functional Materials, Nanjing 210093, China*
[3]*Collaborative Innovation Center of Advanced Microstructures, Nanjing University, Nanjing 210093, China*

(Received 13 August 2021; accepted 16 February 2022; published 4 March 2022; corrected 22 March 2022)

The introduction of non-Hermiticity to topological systems profoundly modifies their topological properties, leading to unprecedented phenomena beyond the descriptions of Bloch band theory, e.g., the breakdown of the conventional bulk-boundary correspondence. However, the comprehensive interplay between band topology and non-Hermiticity remains elusive. Here, based on a non-Hermitian Su-Schrieffer-Heeger model, we demonstrate that in the non-Hermitian topological systems, band topology and non-Hermiticity interplay by competing with each other, exhibiting a transition from symmetry dominance to non-Hermitian dominance. The former is featured with two edge states separately distributed at the two ends of the Su-Schrieffer-Heeger chain, similar to their Hermitian counterparts. In the latter, however, driven by non-Hermiticity, the two edge states become localized toward the same chain end, exhibiting the non-Hermitian skin effect. We find that such a transition is a universal behavior in the non-Hermitian systems, which is responsible for the breakdown of the conventional bulk-boundary correspondence and is the key factor to understanding the non-Hermitian topological properties. Furthermore, it is shown that this transition can be modified by the mode coupling between the edge states. As a comparison, we propose a non-Hermitian square-root Su-Schrieffer-Heeger model, where the edge states do not couple with each other and the mode coupling effect can be deactivated. Our work explicitly reveals the interplay between band topology and non-Hermiticity, which lays the foundation for the studies of non-Hermitian topological physics.

DOI: 10.1103/PhysRevB.105.094103

I. INTRODUCTION

The Hermiticity of a Hamiltonian imposes constraints that guarantee real eigenvalues and orthogonal eigenstates, reflecting the dynamics of an isolated system. In open systems, however, the description of Hermiticity breaks down, while the non-Hermitian Hamiltonians provide suitable approximations to describe their properties [1–5]. Over the past two decades, non-Hermitian physics has been extensively investigated in both theories [6–17] and experiments [18–34], leading to remarkable properties and phenomena such as exceptional features [19,24,27,33], unidirectional invisibility [19,20,23], mode switching [26,32], and enhanced sensitivity [22,31].

Recently, non-Hermiticity has been further shown to fundamentally modify the Bloch band theory, giving rise to unprecedented physics described by non-Bloch band theory [35–39]. Therein, a seminal phenomenon emerges, known as the non-Hermitian skin effect (NHSE) [35]. It describes the intriguing phenomenon that due to the nonreciprocal coupling in non-Hermitian systems, eigenstates of the Hamiltonian collapse and exponentially localize around sample boundaries, exhibiting features similar to the topological edge states in Hermitian systems. Extensive theoretical [40–44] and experimental [45–48] efforts have been made to interpret NHSE.

While NHSE arises from non-Hermiticity and does not necessarily require the system to be topologically nontrivial, in topologically nontrivial systems, it is shown that non-Hermiticity modifies the topological phase transition, leading to the breakdown of the conventional bulk-boundary correspondence (BBC) [35,36,38]. How the band topology and the non-Hermiticity interplay and what the role of NHSE is, however, remain unheeded.

Here, based on a 1D non-Hermitian Su-Schrieffer-Heeger (SSH) model, we demonstrate that in the non-Hermitian topological systems, the band topology and the non-Hermiticity compete with each other, leading to a transition from a band topology (or crystalline symmetry) dominant region (TDR) to a non-Hermiticity dominant region (NHDR) in the parameter space, featuring topological edge states transiting into topological skin modes. As a result, the conventional BBC in the Hermitian limit breaks down and the topological properties are modified in the non-Hermitian systems. We further show that the mode coupling is a vital factor that can affect the TDR-NHDR transition, while in the systems without mode coupling, this effect is deactivated.

*Present address: School of Materials Science and Engineering, Peking University, Beijing 100871, China.
†Author to whom correspondence and requests for materials should be addressed: xiujuanzhang@nju.edu.cn
‡Author to whom correspondence and requests for materials should be addressed: luminghui@nju.edu.cn

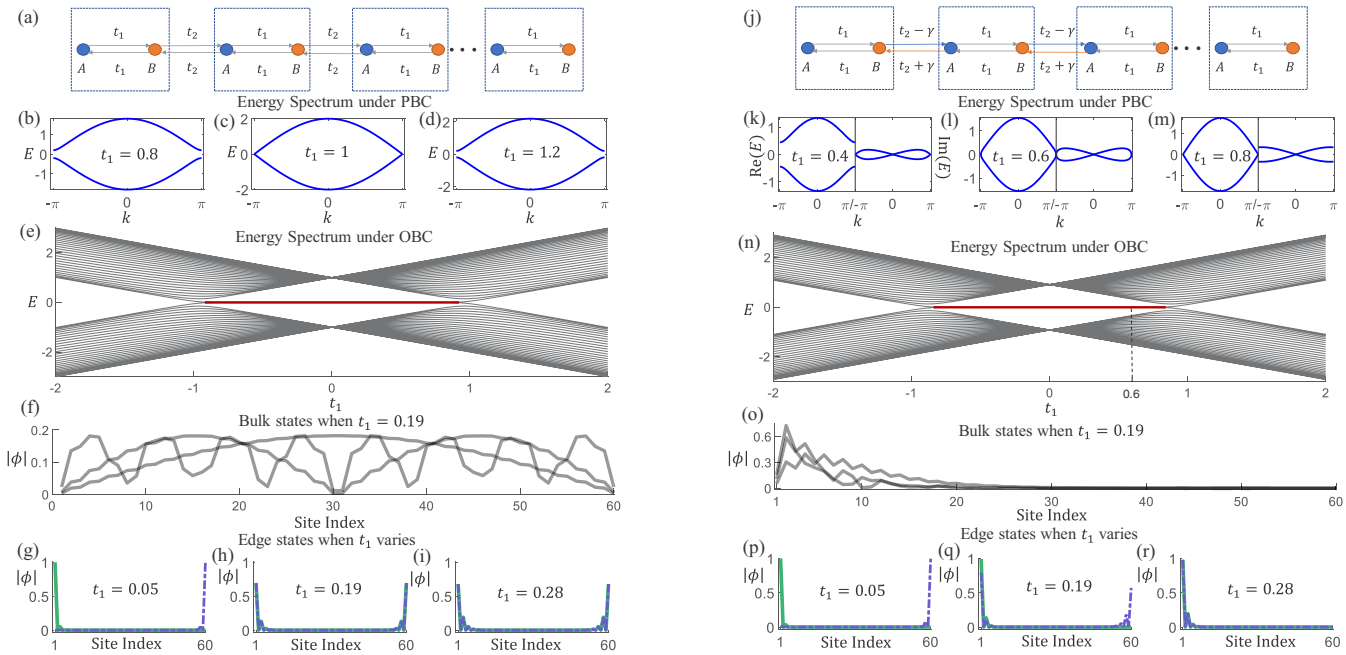

FIG. 1. (a) The Hermitian SSH model. t_1 and t_2 represent the intra- and intercell coupling coefficients. A and B denote the sublattice sites. (b)–(d) Energy spectra under PBC. (e) Energy spectrum under OBC with $N = 30$, with the bulk (edge) states indicated by the black (red) curves. (f)–(i) Mode profiles for three randomly selected bulk states and the two edge states. The gray transparent lines represent the bulk states while the green and purple lines indicate the two edge states. (j) The non-Hermitian SSH model with nonreciprocal intercell coupling, which is characterized by an offset of γ. (k)–(r) Respectively, the same as (b)–(i), only for the non-Hermitian model with $\gamma = 0.4$. Common parameter: $t_2 = 1$.

II. MODEL

We start with a two-band SSH model, as illustrated in Fig. 1(a), whose Hamiltonian is given by

$$H(k) = \begin{pmatrix} 0 & t_1 + t_2 e^{-ik} \\ t_1 + t_2 e^{ik} & 0 \end{pmatrix}, \tag{1}$$

where t_1 (t_2) represents the intra- (inter-) cell coupling coefficient (only the nearest neighbor coupling is considered). k is the Bloch wave vector. This model obeys the chiral (or sublattice) symmetry and presents a Z_2-type topology [39]. As shown in Figs. 1(b)–1(d), where the energy spectra E under periodic boundary condition (PBC) are presented, the energy gap experiences a gap opening-closing-reopening process, predicting a topological phase transition; i.e., when $|t_1| < |t_2|$, the system is topologically nontrivial and hosts edge states with zero energy, while it is trivial for $|t_1| > |t_2|$. $|t_1| = |t_2|$ is the topological transition point. Such a phase diagram is consistent with the topological properties under open boundary condition (OBC) where edge states emerge for $|t_1| < |t_2|$ [see Fig. 1(e); the small discrepancy is due to the finite-size effect]. This is the well-known BBC in Hermitian systems. We show the mode profiles for three randomly selected bulk states and the two edge states in Figs. 1(f)–1(i), which exhibit typical extended or localized behaviors.

When introducing nonreciprocal coupling, the SSH model becomes non-Hermitian [see Fig. 1(j)]. Here, γ is used to characterize the intercell coupling offset. $\gamma = 0$ returns the model to its Hermitian limit. The Hamiltonian for such a non-Hermitian model reads

$$H(k) = \begin{pmatrix} 0 & t_1 + (t_2 - \gamma)e^{-ik} \\ t_1 + (t_2 + \gamma)e^{ik} & 0 \end{pmatrix}. \tag{2}$$

Note that the eigenvalues and eigenvectors of Eq. (2) are not necessarily real. This is the consequence of non-Hermiticity. It is also pointed out that such nonreciprocal coupling induced non-Hermitian systems do not respect parity-time symmetry. We again calculate the energy spectra under PBC and OBC for the non-Hermitian SSH model with $\gamma = 0.4$, as shown in Figs. 1(k)–1(n). Interestingly, the energy gap closing point under PBC [see Fig. 1(l)] is noticeably different from the topological transition points under OBC (where the zero-energy modes disappear). This inconsistence indicates the breakdown of the Hermitian BBC [35,36,38]. Here, we emphasize that such an inconsistence is an indication and a consequence of, but not a reason for the breakdown of the Hermitian BBC. As identified in the following, the physical reason to the breakdown is the competing between the band topology and non-Hermiticity.

We present the mode profiles for three random bulk states in Fig. 1(o), which surprisingly show wave localization toward the left boundary, in sharp contrast to the Hermitian bulk states [see Fig. 1(f)]. This is the manifestation of the so-called NHSE. In fact, driven by non-Hermiticity, all the bulk states become skin modes [35].

For the edge states, however, very different behavior is observed. As shown in Figs. 1(p)–1(r), for smaller t_1, the edge states are localized at both ends of the SSH chain, which are imposed and protected by chiral symmetry that is responsible for the nontrivial band topology. This is the

same as the Hermitian counterpart. With increasing t_1, non-Hermiticity gets stronger and forces the edge states to localize toward the left chain end, competing with the protection of the chiral symmetry. When non-Hermiticity is strong enough, the edge states transit into edge skin modes, as a manifestation of NHSE. We argue that such a competition between band topology (or crystalline symmetry) and non-Hermiticity is exactly the reason that the Hermitian BBC breaks down in non-Hermitian systems, considering the NHSE is only manifested under OBC. As t_1 continuously increases, NHSE becomes overwhelming, topological phase transition happens, and the zero-energy modes disappear.

Note that here there are two kinds of transitions. One is the topological phase transition, which cannot be determined by band gap closing under PBC due to the effect of non-Hermiticity. The other is the transition between band topology (or crystalline symmetry) dominance and non-Hermitian dominance. This transition is *not* considered as a phase transition. It happens because of the competing effect and the zero-energy modes before and after the transition both have topological origin (as shown in the following). In fact, it is this transition that shapes the non-Hermitian topological phase transition.

We notice that the emergence of edge skin modes was also observed previously, known as the consequence of a non-Hermitian coalescence [14]. In Ref. [14], these modes are referred to as the defective edge states. A number-anomalous BBC was proposed to mathematically identify these states [49]. In the present work, we reveal an unambiguous transition between TDR and NHDR behind the emergence of the edge skin modes, which provides a deep physical understanding of this phenomenon and of how it behaves both under thermodynamic limit and in finite structures (as studied in more detail in the following sections). We believe our study, in combination with the previous identifications, would provide a comprehensive understanding of the non-Hermitian topological physics.

III. TRANSITIONS UNDER THERMODYNAMIC LIMIT

In this section, we analytically derive the condition for the transition between TDR and NHDR in the parameter space of (t_1, γ). The zero-energy edge states for the model in Fig. 1(j) are expressed as (see the Supplemental Material [50] for derivations)

$$\phi_{N,\mathrm{A}} = \left(-\frac{t_1}{t_2+\gamma}\right)^{N-1}\phi_{1,\mathrm{A}},$$
$$\phi_{1,\mathrm{B}} = \left(-\frac{t_1}{t_2-\gamma}\right)^{N-1}\phi_{N,\mathrm{B}}. \tag{3}$$

$\phi_{i,j}(i = 1, 2, \ldots, N; j = \mathrm{A}, \mathrm{B})$ represents the wave function on the subsite j in the ith cell. Equation (3) implies that the mode profiles of the edge states are determined by the propagation constants $-\frac{t_1}{t_2+\gamma}$ and $-\frac{t_1}{t_2-\gamma}$. Under the thermodynamic limit (i.e., $N \to \infty$), apply the boundary conditions $\phi_{1,\mathrm{B}} = \phi_{N,\mathrm{A}} = 0$ to Eq. (3), yielding $|t_1| < |t_2 + \gamma|$ and $|t_1| < |t_2 - \gamma|$. For a fixed $t_2 = 1$, these two inequalities enclose a diamond-shaped region in the parameter space of (t_1, γ), i.e., the TDR [orange region in Fig. 2(a)]. In this region, the edge states are separately located at the two ends of the non-Hermitian SSH chain, imposed and protected by the chiral symmetry. Outside the TDR, non-Hermiticity becomes strong enough to destroy the protection of chiral symmetry and the system goes into the NHDR [blue region in Fig. 2(a)]. The transition happens at $|t_1| = |t_2 \pm \gamma|$, where the two edge states become delocalized; i.e., they are not localized at the left chain end nor the right chain end. Instead, they become standing waves, as if there are no edge states. This interesting phenomenon is the result of a balanced effect between band topology and non-Hermiticity.

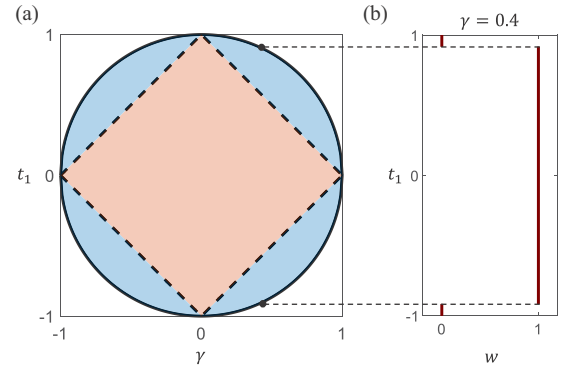

FIG. 2. (a) Diagram for the TDR (orange region) and NHDR (blue region) under thermodynamic limit. The outer circle denotes the topological transition line. To distinguish between the TDR-NHDT transition and the topological phase transition, the former is indicated by dashed lines while the latter is indicated by a solid line. (b) Winding number for the case with $\gamma = 0.4$. Its jumps clearly mark the derived topological transition points.

When the NHSE becomes overwhelming, topological phase transition happens, which demarcates the outer boundary of the NHDR. Here, we adopt a non-Bloch-band theory [35,51] to derive the phase transition points, which are found to locate at $t_1^2 + \gamma^2 = t_2^2$. A non-Hermitian winding number w is also calculated, as shown in Fig. 2(b) for the case with $\gamma = 0.4$, whose jumps are shown to exactly correspond to the derived phase transition points. The non-zero w unambiguously relates the topological nontrivial region to the emergence of the zero-energy modes [see Fig. 1(n), with a discrepancy due to the mode coupling effect]. This indicates that both the edge states and the edge skin modes are topological and have topological robustness. More details on the topological phase transition, the winding number, and the robustness study are shown in the Supplemental Material [50].

IV. EFFECT OF MODE COUPLING

Under the thermodynamic limit, the edge states are separately located at the two ends of the SSH chain without coupling. However, in systems with finite cells, mode coupling between the edge states becomes significant. In this section, we show that the mode coupling can enhance the NHSE and accordingly expand the NHDR. Figure 3(a) presents the TDR-NHDR diagram in a finite non-Hermitian SSH chain with $N = 200$. Without loss of generality, we consider positive coupling coefficients, i.e., $t_1 > 0$ and $\gamma > 0$. TDR and NHDR are quantified by a mode density over the

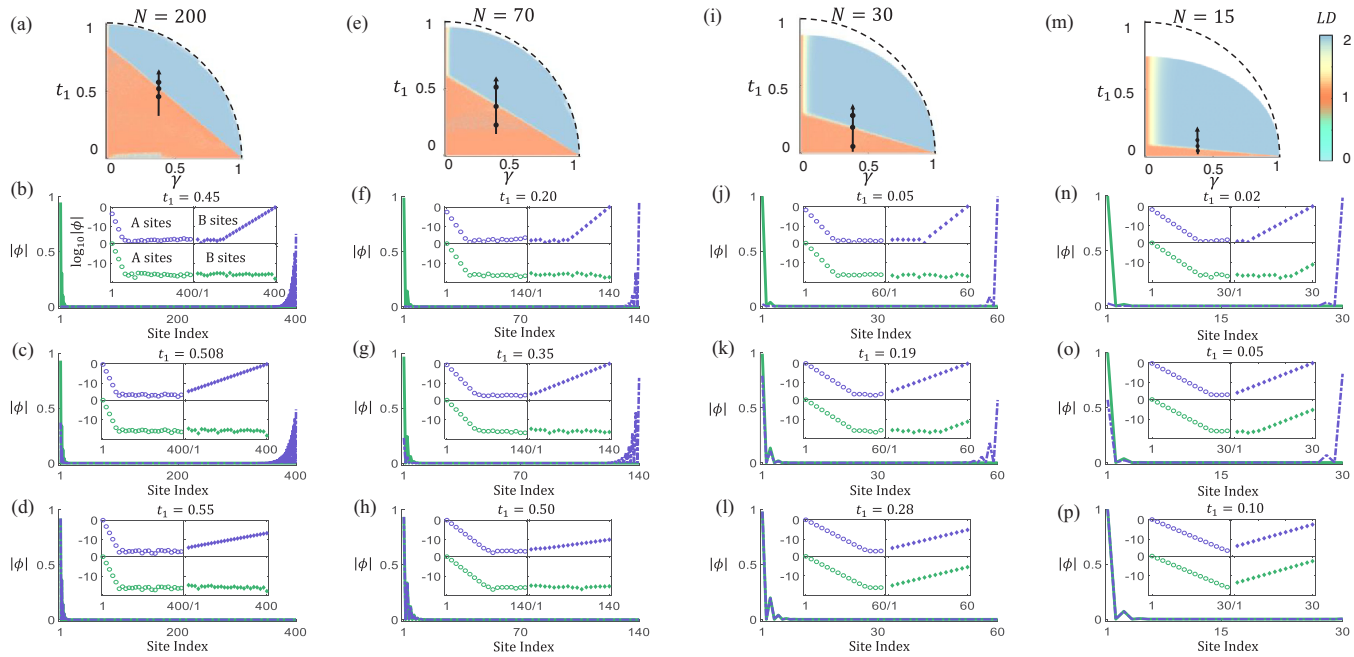

FIG. 3. (a) Numerically calculated TDR-NHDR diagram in a finite non-Hermitian SSH chain with $N = 200$. TDR (orange region) and NHDR (blue region) are characterized by LD = 1 and 2, respectively. The dashed line denotes the topological transition line identified by the non-Bloch-band theory. The solid arrow with dots denotes three examples illustrated in (b)–(d), where the mode profiles for the two zero modes with increasing t_1 are presented (with $\gamma = 0.4$). Insets: the modulus of the wave functions at A and B sites in logarithmic scale, showing energy transfer from right to left during the TDR-NHDR transition. The green and purple lines indicate the two edge (skin) modes. Similar studies are conducted for (e)–(h) $N = 70$, (i)–(l) $N = 30$, and (m)–(p) $N = 15$. Note that the scatter density in the insets is reduced by skipping eight, four, and two sites, respectively, for $N = 200$, 70, and 30.

left-half cells, which is defined as

$$\mathrm{LD} = \sum_{n=1}^{\lfloor N/2 \rfloor} \sum_{i=\mathrm{A,B}} \left[\left|\phi^a_{n,i}\right|^2 + \left|\phi^b_{n,i}\right|^2 \right], \tag{4}$$

where $\lfloor N/2 \rfloor$ rounds down $N/2$ to its next lowest integer. a and b denote the two zero modes. Given that these two modes are square normalized, LD essentially counts the number of localized states at the left chain end, with LD = 1 indicating the two states are separately localized at the two chain ends (marking the TDR) while LD = 2 indicates the two states are localized at the left chain end as non-Hermitian edge skin modes (marking the NHDR).

From Fig. 3(a), it is seen that the transition line separating TDR and NHDR moves away from that in Fig. 2(a) and the NHDR is indeed expanded. In TDR, there are localized states with LD = 0 or 2, indicating they are at the same chain end. Note that these states are not skin modes, instead, they are formed due to the coupling effect. We further present the mode profiles for the two zero modes with increasing t_1 in Figs. 3(b)–3(d), which show evolution similar to that in Figs. 1(p)–1(r); i.e., the two modes transit from edge states to edge skin modes. This further corroborates the results in Fig. 3(a).

We argue that the expansion of NHDR is due to the coupling between the two zero modes. From Eq. (3), it is seen that the left (right) zero mode ϕ^a (ϕ^b) is tightly confined at sites A (B) and exponentially decays toward the right (left) when $N \to \infty$. At finite N, however, ϕ^b starts to leak energy toward the left. Restricted by the boundary condition at the left end, the energy initially in the B sites of ϕ^b is transferred to the A sites of ϕ^a [as shown by the insets in Figs. 3(b)–3(d), the purple dots], indicating ϕ^a and ϕ^b are coupled. Through such a coupling, the NHSE is enhanced and the NHDR is expanded. Note that at finite N, ϕ^a can also transfer energy toward the right to ϕ^b. However, this process is suppressed by the non-Hermiticity and almost all the energy is concentrated in the left [see insets in Figs. 3(b)–3(d), the green dots]. We further present the studies for $N = 70$, 30, and 15. It is shown that with decreasing N, the NHDR is further expanded, owing to a stronger mode coupling. For $N = 15$, the transition line between TDR and NHDR almost touches the x axis, suggesting that in a short chain the NHSE is prominent. Moreover, we find that for near zero γ, the edge states do not transit into the edge skin modes and always exist until the topological phase transition happens [see Figs. 3(a), 3(e), 3(i), and 3(m)]. This indicates that in finite systems with mode coupling, the non-Hermiticity has to be strong enough in order to compete with the band topology. Otherwise, the system behaves as its Hermitian counterpart. It is also pointed out that the topological phase transition line in the finite systems (i.e., the outer boundary of NHDR) deviates from the prediction by non-Bloch-band theory and is size dependent. This is the effect of mode coupling, similar to the finite-size effect in Hermitian systems.

V. A NON-HERMITIAN SQUARE-ROOT SSH MODEL

In this section, we propose a non-Hermitian square-root SSH model to demonstrate the TDR-NHDR transition

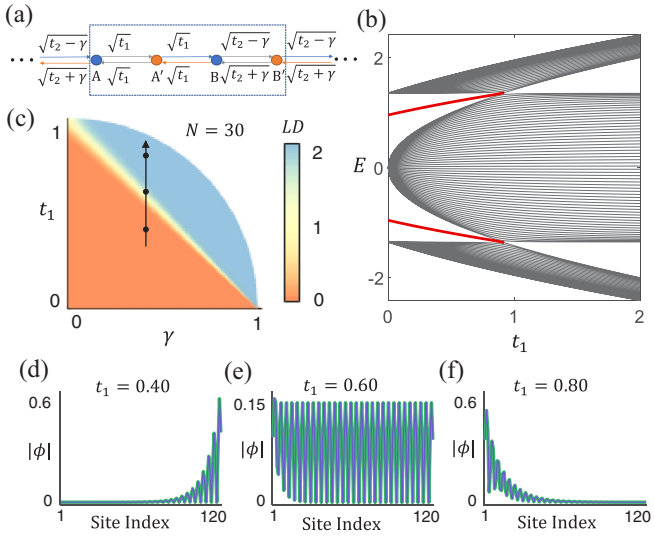

FIG. 4. (a) The square-root non-Hermitian SSH model. t_1, t_2, and γ denote the same coupling coefficients in the non-Hermitian SSH model, except that in the square-root model, the coupling coefficients are taken as a square-root operation. A, A′, B, and B′ represent the four sites. (b) The energy spectrum of the square-root model under OBC. The bulk states are indicated by the black lines. The edge (skin) states are indicated by the red lines, which show that in the square-root model, the edge (skin) states are split symmetric to zero energy. (c) Numerically calculated diagram for TDR (LD = 0, the orange color) and NHDR (LD = 2, the blue color) in the finite chain. The black arrow with dots indicates three examples illustrated in (d)–(f), where the mode profiles of the two edge (skin) states with increasing t_1 are presented, exhibiting the TDR-NHDR transition. The green and purple solid lines denote the two states. A delocalization occurs at the transition line (i.e., $t_1 = 0.6$). Common parameters: $t_2 = 1$, $\gamma = 0.4$, and $N = 30$.

without mode coupling. The square-root model takes a square-root operation on the Hamiltonian of the parent model by adding a set of subsites on wherever hopping is permitted [52–55]. As shown in Fig. 4(a), this model modifies the hopping coefficients of the original SSH model to be square rooted, obeying the following Hamiltonian:

$$H(k) = \begin{pmatrix} 0 & \sqrt{t_1} & 0 & \sqrt{t_2-\gamma}\,e^{-ik} \\ \sqrt{t_1} & 0 & \sqrt{t_1} & 0 \\ 0 & \sqrt{t_1} & 0 & \sqrt{t_2+\gamma} \\ \sqrt{t_2+\gamma}\,e^{ik} & 0 & \sqrt{t_2-\gamma} & 0 \end{pmatrix}. \tag{5}$$

We calculate the eigenspectra of a finite chain with $N = 30$, as shown in Fig. 4(b). The edge states in the square-root model are split, with positive and negative energy symmetric to the zero energy (see the red lines) and can be expressed as (see the Supplemental Material [50] for the derivations, as well as the discussions on the topological phase transition and the winding number)

$$\phi_{n,\mathrm{A}} = 0, \quad \phi_{1,j} = \left(-\frac{t_1}{t_2-\gamma}\right)^{N-1} \phi_{N,j},$$

with

$$j = \mathrm{A}',\ \mathrm{B},\ \mathrm{B}' \quad \text{for} \quad \left|\frac{t_1}{t_2-\gamma}\right| < 1. \tag{6}$$

From Eq. (6) (see the Supplemental Material [50] for the full solution), it is seen that the edge states in the square-root model are localized at the same chain end, i.e., the right end. This is due to the reduction of the inversion symmetry. A direct consequence is that the two edge states in this case are no longer coupled with each other. Accordingly, the NHDR expansion is deactivated. In Fig. 4(c), we present the TDR-NHDR diagram at a finite $N = 30$, which shows that the transition line lies at $t_1 = t_2 - \gamma$, exactly the same as that in the thermodynamic limit. The mode profiles for the two localized states with increasing t_1 are presented in Figs. 4(d)–4(f). A similar evolution as the SSH model is observed as the two states transit from the edge states located at the right end to the edge skin modes located at the left end. Interestingly, due to the lack of coupling effect, the delocalization behavior at the transition line, as discussed for the SSH model under the thermodynamic limit, is restored in the square-root model, where the two edge states become extended Bloch waves [see Fig. 4(e)]. In the finite SSH model, however, this phenomenon is absent due to the coupling effect.

VI. CONCLUSIONS

Based on a non-Hermitian SSH model, we demonstrate in non-Hermitian systems that the band topology and non-Hermiticity interplay by competing with each other, leading to an unambiguous transition from band-topology dominance to non-Hermitian dominance, which shapes the non-Hermitian topological phase transition. We further find that the mode coupling between the edge states can be a positive aid to enhance the NHSE, which can be activated or deactivated in different systems. Our work reveals the fundamental interplay between band topology and non-Hermiticity, which can serve as a universal mechanism for the non-Hermitian topological physics. The results can be generalized to a variety of physical fields, as well as to the higher dimensions, where the chapters for non-Hermitian physics are to be opened (see the Supplemental Material [50] for our discussions on non-Hermitian skin effect in higher dimensions and its competing effect with band topology, where a square lattice [56] and a Kagome lattice [57–59] are demonstrated as examples). They also apply to non-Hermitian systems with bipolar skin effect that corresponds to a phenomenon where the eigenstates with different eigenenergy can localize toward different open boundaries [37]. Driven by the competing effect, topological states in these systems also experience the TDR-NHDR transition with the localization of the resultant edge skin modes dependent on what eigenenergy they fall onto. Experimentally, our results can be implemented in systems with nonreciprocal coupling [45–48].

ACKNOWLEDGMENTS

This work is supported by the National Key R&D Program of China (Grants No. 2017YFA0303702 and No. 2018YFA0306200), the National Natural Science Foundation of China (Grants No. 51902151, No. 11625418, and No. 51732006), and the Natural Science Foundation of Jiangsu Province (Grant No. BK20190284).

[1] H. J. Carmichael, Phys. Rev. Lett. **70**, 2273 (1993).
[2] N. Hatano and D. R. Nelson, Phys. Rev. Lett. **77**, 570 (1996).
[3] S. Diehl, E. Rico, M. A. Baranov, and P. Zoller, Nat. Phys. **7**, 971 (2011).
[4] T. Eichelkraut, R. Heilmann, S. Weimann, S. Stützer, F. Dreisow, D. N. Christodoulides, S. Nolte, and A. Szameit, Nat. Commun. **4**, 2533 (2013).
[5] S. Malzard, C. Poli, and H. Schomerus, Phys. Rev. Lett. **115**, 200402 (2015).
[6] C. M. Bender and S. Boettcher, Phys. Rev. Lett. **80**, 5243 (1998).
[7] C. M. Bender, D. C. Brody, and H. F. Jones, Phys. Rev. Lett. **89**, 270401 (2002).
[8] C. M. Bender, Rep. Prog. Phys. **70**, 947 (2007).
[9] A. Mostafazadeh, Phys. Rev. Lett. **99**, 130502 (2007).
[10] K. G. Makris, R. El-Ganainy, D. N. Christodoulides, and Z. H. Musslimani, Phys. Rev. Lett. **100**, 103904 (2008).
[11] M. S. Rudner and L. S. Levitov, Phys. Rev. Lett. **102**, 065703 (2009).
[12] K. Esaki, M. Sato, K. Hasebe, and M. Kohmoto, Phys. Rev. B **84**, 205128 (2011).
[13] A. Szameit, M. C. Rechtsman, O. Bahat-Treidel, and M. Segev, Phys. Rev. A **84**, 021806(R) (2011).
[14] T. E. Lee, Phys. Rev. Lett. **116**, 133903 (2016).
[15] Z. Gong, Y. Ashida, K. Kawabata, K. Takasan, S. Higashikawa, and M. Ueda, Phys. Rev. X **8**, 031079 (2018).
[16] F. K. Kunst, E. Edvardsson, J. C. Budich, and E. J. Bergholtz, Phys. Rev. Lett. **121**, 026808 (2018).
[17] H. Shen, B. Zhen, and L. Fu, Phys. Rev. Lett. **120**, 146402 (2018).
[18] Y. Choi, S. Kang, S. Lim, W. Kim, J.-R. Kim, J.-H. Lee, and K. An, Phys. Rev. Lett. **104**, 153601 (2010).
[19] A. Regensburger, C. Bersch, M.-A. Miri, G. Onishchukov, D. N. Christodoulides, and U. Peschel, Nature (London) **488**, 167 (2012).
[20] X. Zhu, L. Feng, P. Zhang, X. Yin, and X. Zhang, Opt. Lett. **38**, 2821 (2013).
[21] T. E. Lee and C.-K. Chan, Phys. Rev. X **4**, 041001 (2014).
[22] H. Hodaei, M.-A. Miri, M. Heinrich, D. N. Christodoulides, and M. Khajavikhan, Science **346**, 975 (2014).
[23] S. Longhi, Opt. Lett. **40**, 5694 (2015).
[24] B. Zhen, C. W. Hsu, Y. Igarashi, L. Lu, I. Kaminer, A. Pick, S.-L. Chua, J. D. Joannopoulos, and M. Soljačić, Nature (London) **525**, 354 (2015).
[25] L. Feng, R. El-Ganainy, and L. Ge, Nat. Photonics **11**, 752 (2017).
[26] S. Ke, B. Wang, H. Long, K. Wang, and P. Lu, Opt. Quantum Electron. **49**, 224 (2017).
[27] W. Hu, H. Wang, P. P. Shum, and Y. D. Chong, Phys. Rev. B **95**, 184306 (2017).
[28] L. Xiao, X. Zhan, Z. H. Bian, K. K. Wang, X. Zhang, X. P. Wang, J. Li, K. Mochizuki, D. Kim, N. Kawakami *et al.*, Nat. Phys. **13**, 1117 (2017).
[29] T. Yoshida, R. Peters, and N. Kawakami, Phys. Rev. B **98**, 035141 (2018).
[30] M. Pan, H. Zhao, P. Miao, S. Longhi, and L. Feng, Nat. Commun. **9**, 1308 (2018).
[31] M. P. Hokmabadi, A. Schumer, D. N. Christodoulides, and M. Khajavikhan, Nature (London) **576**, 70 (2019).
[32] S. Assawaworrarit and S. Fan, Nat. Electron. **3**, 273 (2020).
[33] B. Midya, H. Zhao, and L. Feng, Nat. Commun. **9**, 2674 (2018).
[34] H. Zhao, X. Qiao, T. Wu, B. Midya, S. Longhi, and L. Feng, Science **365**, 1163 (2019).
[35] S. Yao and Z. Wang, Phys. Rev. Lett. **121**, 086803 (2018).
[36] S. Yao, F. Song, and Z. Wang, Phys. Rev. Lett. **121**, 136802 (2018).
[37] F. Song, S. Yao, and Z. Wang, Phys. Rev. Lett. **123**, 246801 (2019).
[38] K. Yokomizo and S. Murakami, Phys. Rev. Lett. **123**, 066404 (2019).
[39] K. Kawabata, K. Shiozaki, M. Ueda, and M. Sato, Phys. Rev. X **9**, 041015 (2019).
[40] K. Zhang, Z. Yang, and C. Fang, Phys. Rev. Lett. **125**, 126402 (2020).
[41] Z. Yang, K. Zhang, C. Fang, and J. Hu, Phys. Rev. Lett. **125**, 226402 (2020).
[42] K. Kawabata, M. Sato, and K. Shiozaki, Phys. Rev. B **102**, 205118 (2020).
[43] X. Zhu, H. Wang, S. K. Gupta, H. Zhang, B. Xie, M. Lu, and Y. Chen, Phys. Rev. Res. **2**, 013280 (2020).
[44] S. Longhi, Opt. Lett. **45**, 5250 (2020).
[45] S. Weidemann, M. Kremer, T. Helbig, T. Hofmann, A. Stegmaier, M. Greiter, R. Thomale, and A. Szameit, Science **368**, 311 (2020).
[46] L. Xiao, T. Deng, K. Wang, G. Zhu, Z. Wang, W. Yi, and P. Xue, Nat. Phys. **16**, 761 (2020).
[47] X. Zhang, Y. Tian, J.-H. Jiang, M.-H. Lu, and Y.-F. Chen, Nat. Commun. **12**, 5377 (2021).
[48] L. Zhang, Y. Yang, Y. Ge, Y.-J. Guan, Q. Chen, Q. Yan, F. Chen, R. Xi, Y. Li, D. Jia *et al.*, Nat. Commun. **12**, 6297 (2021).
[49] X.-R. Wang, C.-X. Guo, and S.-P. Kou, Phys. Rev. B **101**, 121116(R) (2020).
[50] See Supplemental Material at http://link.aps.org/supplemental/10.1103/PhysRevB.105.094103 for derivations of the edge states, discussions on the topological phase transition, and the winding number for both the non-Hermitian SSH model and the non-Hermitian square-root SSH model. The discussions for non-Hermitian skin effect in higher dimensions and its competing effect with band topology are also included. The references referred to in the Supplemental Material are Refs. [35,38,51,54,56–59].
[51] K. Yokomizo and S. Murakami, Prog. Theor. Exp. Phys. **2020**, 12A102 (2020).
[52] J. Arkinstall, M. H. Teimourpour, L. Feng, R. El-Ganainy, and H. Schomerus, Phys. Rev. B **95**, 165109 (2017).
[53] T. Mizoguchi, Y. Kuno, and Y. Hatsugai, Phys. Rev. A **102**, 033527 (2020).
[54] M. Ezawa, Phys. Rev. Res. **2**, 033397 (2020).
[55] Z. Lin, S. Ke, X. Zhu, and X. Li, Opt. Express **29**, 8462 (2021).
[56] B.-Y. Xie, H.-F. Wang, H.-X. Wang, X.-Y. Zhu, J.-H. Jiang, M.-H. Lu, and Y.-F. Chen, Phys. Rev. B **98**, 205147 (2018).
[57] X. Ni, M. A. Gorlach, A. Alu, and A. B. Khanikaev, New J. Phys. **19**, 055002 (2017).
[58] H. Xue, Y. Yang, F. Gao, Y. Chong, and B. Zhang, Nat. Mater. **18**, 108 (2019).
[59] X. Ni, M. Weiner, A. Alu, and A. B. Khanikaev, Nat. Mater. **18**, 113 (2019).

Correction: The first name of the first author had a typographical error and has been fixed.